Crystal Structures of the *Toxoplasma gondii* Hypoxanthine-Guanine Phosphoribosyltransferase−GMP and −IMP Complexes: Comparison of Purine Binding Interactions with the XMP Complex[†,‡]

Annie Héroux, E. Lucile White, Larry J. Ross, and David W. Borhani*

Drug Discovery Division, Southern Research Institute, Birmingham, Alabama 35205

Received March 3, 1999; Revised Manuscript Received July 14, 1999

ABSTRACT: The crystal structures of the guanosine 5′-monophosphate (GMP) and inosine 5′-monophosphate (IMP) complexes of *Toxoplasma gondii* hypoxanthine-guanine phosphoribosyltransferase (HGPRT) have been determined at 1.65 and 1.90 Å resolution. These complexes, which crystallize in space groups $P2_1$ ($a = 65.45$ Å, $b = 90.84$ Å, $c = 80.26$ Å, and $\beta = 92.53°$) and $P2_12_12_1$ ($a = 84.54$ Å, $b = 102.44$ Å, and $c = 108.83$ Å), each comprise a tetramer in the crystallographic asymmetric unit. All active sites in the tetramers are fully occupied by the nucleotide. Comparison of these structures with that of the xanthosine 5′-monophosphate (XMP)−pyrophosphate−Mg^{2+} ternary complex reported in the following article [Héroux, A., et al. (1999) *Biochemistry 38*, 14495−14506] shows how *T. gondii* HGPRT is able to recognize guanine, hypoxanthine, *and* xanthine as substrates, and suggests why the human enzyme cannot use xanthine efficiently. Comparison with the apoenzyme reveals the structural changes that occur upon binding of purines and ribose 5′-phosphate to HGPRT. Two structural features important to the HGPRT mechanism, a previously unrecognized active site loop (loop III′, residues 180−184) and an active site peptide bond (Leu78−Lys79) that adopts both the cis and the trans configurations, are presented.

Encephalitis caused by the apicomplexan protozoan *Toxoplasma gondii* is the second-leading cause of death among patients with acquired immune deficiency syndrome (AIDS)[1] (*1*, *2*). New and more potent drugs are urgently needed to treat these infections (*3*). Parasitic protozoa, including those of the genus *Toxoplasma*, cannot carry out the de novo synthesis of purine nucleotides required for growth and replication. Instead, the parasites salvage preformed purine bases from the host (*4*, *5*). Purine salvage funnels through the enzyme hypoxanthine-guanine phosphoribosyltransferase (HGPRT, EC 2.4.2.8), which catalyzes the Mg^{2+}-dependent conversion of hypoxanthine, guanine, or xanthine and α-D-5-phosphoribosyl-1-pyrophosphate (PRPP) to purine nucleotides and inorganic pyrophosphate (Scheme 1). HGPRT has long been recognized as a chemotherapeutic target for malaria, giardiasis, trypanosomiasis, and toxoplasmosis (*6*, *7*). Selective inhibition of the protozoal HGPRT is critical, however, since HGPRT deficiency in humans causes severe gouty arthritis or uric acid nephrolithiasis (*8*), or neonatally the devastating neurological syndrome described by Lesch and Nyhan (*9*). Therefore, understanding differences in substrate specificity between human and protozoal HGPRTs is fundamental to the design of selective HGPRT inhibitors that are useful for the treatment of protozoal diseases (*6*). Despite the determination of many crystal structures of both human (*10*−*12*) and protozoal (*13*−*16*) HGPRTs, however, the mechanisms by which protozoal HGPRTs are able, unlike the human enzyme, to catalyze the efficient conversion of xanthine to xanthosine 5′-monophosphate (XMP) have not been clarified.

We report here and in the following article (*17*) the crystal structures of *T. gondii* HGPRT with guanosine 5′-monophosphate (GMP), inosine 5′-monophosphate (IMP), and XMP−pyrophosphate−Mg^{2+} bound in the active site. These structures are at significantly higher resolution (1.65, 1.90, and 1.60 Å, respectively) than that of the *T. gondii* HGPRT apoenzyme (2.4 Å) reported previously (*16*). Furthermore, in each of our structures, every active site of the HGPRT tetramer is fully occupied by the nucleotide.

As our structures are the first reported for a protozoal HGPRT in complex with all three nucleotide products, we describe here the structural features that allow *T. gondii*

[†] This work was supported in part by NIH Grants AI39952 (D.W.B.) and AI30279 (James R. Piper) and by Southern Research Institute Internal Research and Development Grant 8349 (D.W.B.).

[‡] The atomic coordinates and observed structure factors for the GMP and IMP complexes have been deposited in the Protein Data Bank with accession numbers 1qk3, r1qk3sf, 1qk4, and r1qk4sf, respectively. The atomic coordinates and the observed structure factors for the XMP−pyrophosphate−Mg^{2+} complex (see ref *17*) have accession numbers 1qk5 and r1qk5sf.

* To whom correspondence should be addressed: Department of Organic Chemistry, Southern Research Institute, 2000 Ninth Ave. S., Birmingham, AL 35205. E-mail: borhani@sri.org. Phone: (205) 581-2555. Fax: (205) 581-2877.

[1] Abbreviations: AIDS, acquired immune deficiency syndrome; DTT, dithiothreitol; EDTA, ethylenediaminetetraacetic acid; GMP, guanosine 5′-monophosphate; HGPRT, hypoxanthine-guanine phosphoribosyltransferase; $HGPRT_{Apo}$, *T. gondii* HGPRT−apoenzyme structure; $HGPRT_{GMP}$, *T. gondii* HGPRT−GMP complex structure; $HGPRT_{IMP}$, *T. gondii* HGPRT−IMP complex structure; $HGPRT_{XMP-PP_i-Mg}$, *T. gondii* HGPRT−XMP−pyrophosphate−Mg^{2+} complex structure; IMP, inosine 5′-monophosphate; PEG, polyethylene glycol; PMSF, phenylmethanesulfonyl fluoride; PP_i, pyrophosphate; PRPP, α-D-5-phosphoribosyl 1-pyrophosphate; PRTase, phosphoribosyltransferase; XGPRT, xanthine-guanine phosphoribosyltransferase; XMP, xanthosine 5′-monophosphate.

10.1021/bi990507q CCC: $18.00
Published on Web 10/15/1999

Scheme 1

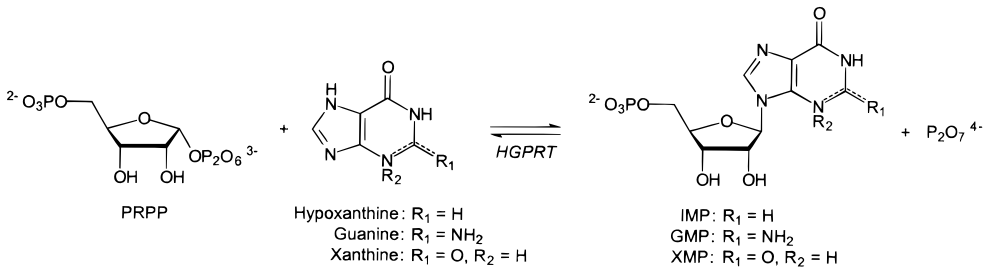

HGPRT to bind guanine, hypoxanthine, and xanthine in the active site. Comparison with the structures of human HGPRT suggests why that enzyme cannot use xanthine efficiently. We also discuss the structural changes that occur upon binding of purines and ribose 5′-phosphate to the apoenzyme. Finally, we describe a previously unrecognized active site loop, an active site peptide bond that adopts either the cis or the trans configuration, and the exchange of the largest active site loop between subunits in the HGPRT tetramer.

EXPERIMENTAL PROCEDURES

HGPRT Expression and Purification

Expression. The cloning of *T. gondii* HGPRT has been described previously (*18*, *19*). Overexpression of the enzyme was accomplished in *Escherichia coli*, using plasmid pETC1 (a derivative of pET15b; Novagen) (*20*). A single colony of *E. coli* BL21(DE3)/pETC1 was inoculated into 5 mL of 2× YT medium (16 g/L tryptone, 10 g/L yeast extract, and 5 g/L NaCl) containing 100 mg/L ampicillin and grown overnight while it was shaken (250 rpm) at 37 °C. This culture (2.5 mL) was diluted into 500 mL of medium, and shaken at 37 °C. When the culture had reached an OD_{600} of ∼0.8, expression of HGPRT was induced by the addition of isopropyl β-D-thiogalactoside (final concentration of 1 mM). Cells were harvested 3 h later by centrifugation, washed with phosphate-buffered saline, repelleted, and stored at −80 °C.

Purification. All procedures were performed at 4 °C. The frozen cell pellet from 1 L of *E. coli* culture was resuspended in 20 mL of 50 mM Tris-HCl (pH 8.0), 10 mM $MgCl_2$, 20 mM KCl, 2 mM phenylmethanesulfonyl fluoride (PMSF), 4 μg/mL pepstatin A, 4 μg/mL leupeptin, 1 mM benzamidine, 20 μg/mL soybean trypsin inhibitor, and 1 mM PRPP and then extracted by two passes through a French press at 15 000−20 000 lb/in.^{2}. The sample was clarified by centrifugation at 27000*g* for 20 min and then applied to a Ni^{2+}−agarose cartridge (Pharmacia) equilibrated with 10 mM imidazole, 500 mM NaCl, and 20 mM sodium phosphate (pH 7.4−7.6). The column was washed with 15 mL of equilibration buffer containing 150 mM imidazole. Recombinant HGPRT was eluted from the column with 5 mL of equilibration buffer containing 1000 mM imidazole. PMSF and 1,10-phenanthroline were added (2 mM each) to the eluate, which was then immediately passed over Sephadex G-25 columns (PD-10, Pharmacia Biotech) equilibrated with 25 mM Tris-HCl (pH 8.0), 10 mM $MgCl_2$, 100 mM KCl, 1 mM dithiothreitol (DTT), and 0.1 mM ethylenediaminetetraacetic acid (EDTA). Pooled fractions were supplemented with 1 mM PRPP. The N-terminal His_6 tag was removed by overnight digestion on ice with thrombin (Sigma catalog no. T-3010; 4 units/mL HGPRT); digestion was halted by addition of PMSF. The sample was then applied to a preparative gel filtration column (Pharmacia HiLoad 26/60 Superdex 200 prepgrade) equilibrated with 25 mM Tris-HCl (pH 8.0), 10 mM $MgCl_2$, 100 mM KCl, 1 mM DTT, 0.1 mM EDTA, and 10% glycerol. Active fractions were pooled, concentrated (Millipore BioMax 15-10000) to ∼20 mg/mL, and stored at 4 °C. Enzyme for use in kinetics studies was stored at −20 °C [glycerol added to a final concentration of 50% (v/v)].

Miscellaneous. HGPRT activity was assayed spectrophotometrically (*21*) at 37 °C in 100 mM Tris-HCl (pH 8.0), 20 mM $MgCl_2$, 0.1 mM EDTA, 0.1 mg/mL bovine serum albumin, purine base (80 μM guanine or hypoxanthine and 500 μM xanthine), and PRPP (500 μM for guanine and hypoxanthine and 2 mM for xanthine). The increase in absorbance at 244.0, 257.4, and 252.0 nm was converted to HGPRT activity using extinction coefficient changes (determined from the extinction coefficients for base and nucleotide in assay buffer) of 2620, 4894, and 4416 M^{-1} cm^{-1} for hypoxanthine, guanine, and xanthine, respectively. Discontinuous sodium dodecyl sulfate−polyacrylamide gel electrophoresis was used to assess the purity of the recombinant HGPRT and to determine the subunit molecular weight (*22*). Protein concentrations were determined by the Bradford procedure (*23*), using bovine γ globulin as the standard.

Crystallization and Data Collection

Crystallization. A preliminary crystallization screen (*24*, *25*) with the Crystal Screen Kit (Hampton Research) under vapor diffusion conditions at 4 °C yielded two conditions. The optimal conditions were (1) 15 to 20% polyethylene glycol (PEG) 8000, 100 mM potassium phosphate (pH 5.0−6.0), and 0.25% octyl β-D-glucopyranoside and (2) 30% PEG 4000, 100 mM Tris-HCl (pH 8.5), and 200 mM Li_2SO_4. *T. gondii* HGPRT (10−20 mg/mL) containing 1 mM GMP or IMP was mixed with an equal volume of the precipitant and equilibrated against the precipitant at 4 °C (hanging drops). Prismatic crystals (space group $P2_1$, $a = 65.45$ Å, $b = 90.84$ Å, $c = 80.26$ Å, and $\beta = 92.53°$) formed at low pH (5−6) in the presence of GMP. Thin, plate-like crystals (space group $P2_12_12_1$, $a = 84.54$ Å, $b = 102.44$ Å, and $c = 108.83$ Å) formed at pH 8.5 in the presence of IMP. Crystals were harvested into mother liquors containing an increased concentration of PEG (40%) and up to 30% glycerol as a cryoprotectant, and were then flash-cooled in liquid nitrogen.

Data Collection and Processing. X-ray diffraction data were collected at the Cornell High Energy Synchrotron Source (beamline A1, $\lambda = 0.908$ Å, ADSC Quantum-1 CCD

Table 1: Data Collection and Refinement Statistics

	GMP	IMP
Crystal Parameters		
space group	$P2_1$	$P2_12_12_1$
a (Å)	65.45	84.54
b (Å)	90.84	102.44
c (Å)	80.26	108.83
β (deg)	92.53	
volume (Å^3)	476733	894150
no. of subunits per asymmetric unit	4	4
Data Collection Statistics		
resolution range (Å)	12.5−1.65	12.5−1.90
no. of observations	302104	305699
no. of unique reflections	108535	74791
mosaicity (deg)	0.45	0.5
overall		
R_{sym} (%)	5.3	7.6
I/σ_I	9.4	10.7
data completeness (%)	96.4	99.6
mean multiplicity	2.8	4.1
highest-shell		
resolution range (Å)	1.71−1.65	1.97−1.90
R_{sym} (%)	45.9	38.3
I/σ_I	1.7	3.5
data completeness (%)	85.3	100.0
mean multiplicity	2.0	4.0
Refinement Statistics		
no. of reflections used in R_{cryst} ($F > 0\sigma_F$)	103103	70933
no. of reflections used in R_{free} ($F > 0\sigma_F$)	5403	3778
R_{cryst} (%)	20.2	18.9
R_{free} (%)	23.1	23.8
rmsd for bond lengths (Å)	0.014	0.014
rmsd for bond angles (deg)	1.5	1.8
Ramachandran plot (% allowed, generously allowed, and disallowed residues)	98.3, 0.9, 0.8	99.0, 1.0, 0.0
no. of atoms [protein (including alternate conformations), ligand, water]	7279, 96, 645	7106, 92, 485
average *B*-factors (Å^2) (protein, ligand, water)	21.7, 18.2, 29.0	22.5, 21.1, 26.0

detector, GMP complex) and the Stanford Synchrotron Radiation Laboratory (beamline 7-1, $\lambda = 1.080$ Å, MAR Research image plate detector, IMP complex) by the rotation method (0.5−1.0°, exposure for 30−120 s) at 100 K. Data processing was performed with the CCP4 suite of programs (*26*). Crystal orientations were determined with REFIX (*27*) and refined with IDXREF. The diffraction data (Table 1) were integrated with MOSFLM (*28*), scaled and merged with SCALA (*29*), and placed on an absolute scale with TRUNCATE (*30*).

Structure Determination

$HGPRT_{GMP}$. The self-rotation function (AMORE) (*31*) revealed the presence of four HGPRT subunits in the asymmetric unit related by 222 symmetry. The structure was determined by molecular replacement, using human HGPRT (one subunit of the tetramer, without GMP or water molecules) as the search model (*10*). The cross-rotation function (AMORE) yielded four strong peaks consistent with the noncrystallographic symmetry. The translation function (TFFC) (*32*) was much less clear, but nonetheless allowed placement of the four HGPRT subunits as a compact tetramer (correlation coefficient of 40%, 12.5−2.5 Å). Four-fold noncrystallographic symmetry averaging and solvent flattening (DM) (*33*) improved the electron density map such that a model could be built (O) (*34*). Refinement (X-PLOR) (35) lowered the *R*-factor a few percent, but then stalled. Recalculation of the translation function with the refined model indicated that the entire tetramer needed to be shifted by approximately 1 Å. X-PLOR refinement (with noncrystallographic symmetry constraints, then restraints), model rebuilding, and refinement with REFMAC (*36*) and ARP (*37*) provided the final model, the quality of which was assessed with PROCHECK (*38*), WHATIF (*39*), and WHATCHECK (*40*). The refinement is summarized in Table 1. The model comprises 893 HGPRT amino acids (out of the 920 possible), two Gly-Ser-His N-terminal peptides (a remnant of the pET15b vector) for subunits B and C, and four GMP and 645 water molecules. Residues at the C-terminus (residues 229 and 230 in subunits A and B, and residue 230 in subunits C and D), loop II in subunit C (residues 116−132), and loop III′ in subunits C and D (residues 183 and 184) were not located. The quality of the data permitted the identification of alternate conformations for several side chains. The Ramachandran plot indicated that Ser103 and Ser104 in subunit C, and Cys203 in all four subunits, were in the disallowed region. While the first two residues lay in weak electron density, residue 203 was in clear, strong density.

$HGPRT_{IMP}$. The self-rotation function revealed the presence of four HGPRT subunits in the asymmetric unit, again related by 222 symmetry. The structure was determined by molecular replacement, using $HGPRT_{GMP}$ subunit A as the search model (without solvent, GMP, or loop II residues A114−A133; correlation coefficient of 25%, 12.5−2.5 Å). Noncrystallographic symmetry averaging and refinement proceeded more smoothly than for $HGPRT_{GMP}$ (Table 1). Alternate conformations were found for several side chains, and the cis peptide bond between residues Leu78 and Lys79 was clearly apparent in $2F_o - F_c$ and $F_o - F_c$ maps. The final model has 880 amino acids and four IMP and 485 water molecules. Residues 120−124 and 230 in subunits A and B, residues 1, 117−131, and 230 in subunit C, and residues 117−125, 182, and 183 in subunit D were not located. Figures were prepared with RIBBONS (*41*).

RESULTS AND DISCUSSION

Recombinant *T. gondii* HGPRT was overexpressed in *E. coli* and purified to apparent homogeneity. Analytical gel filtration showed unequivocally that the enzyme, like human HGPRT, was a tetramer, not a dimer of dimers as suggested previously (*16*). The oligomeric state of the enzyme was unchanged from pH 5.5 to 8.0. Recombinant *T. gondii* HGPRT had specific enzymatic activities at pH 8.0 and 37 °C of 17.1, 28.6, and 69.7 μmol min^{-1} mg^{-1} with hypoxanthine, guanine, and xanthine as the substrate, respectively. Its enzymatic activity at pH 5 was approximately 4% of that observed at pH 8.

The structures of the GMP ($HGPRT_{GMP}$) and IMP ($HGPRT_{IMP}$) complexes of *T. gondii* HGPRT were determined and refined at 1.65 and 1.90 Å resolution, respectively; the structure determination is summarized in Table 1. In both structures, clear electron density was present for the entire nucleotide in all four active sites of the tightly associated HGPRT tetramer in the crystallographic asymmetric unit. The structure of the XMP−pyrophosphate−Mg^{2+} ternary complex ($HGPRT_{XMP-PP_i-Mg}$) is reported at 1.60 Å resolution in the following article (*17*). Our structures were determined using synchrotron data collected under cryogenic conditions,

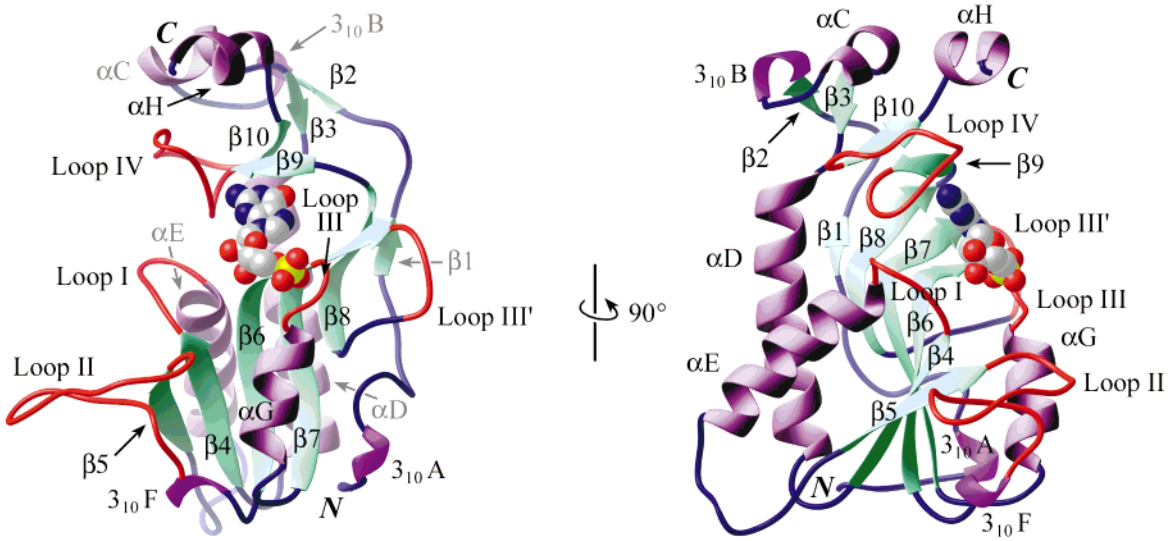

FIGURE 1: RIBBONS (*41*) diagram of the *T. gondii* $HGPRT_{GMP}$ subunit. GMP is shown as a space-filling model in the active site, located between the upper hood domain and the large lower core domain. Helices are lavender, β-strands green, and the five active site loops red.

and thus are at a much higher resolution than the apoenzyme structure ($HGPRT_{Apo}$ at 2.4 Å resolution) (*16*).

The secondary structure of nucleotide-bound *T. gondii* HGPRT is similar to that of other HGPRTs (Figure 1). HGPRT consists of two domains, the "core" (doubly wound α/β-sheet) and the "hood" (twisted β-sandwich). The active site, at the junction of the two domains, is surrounded by several flexible loops. The purine ring of the nucleotides is bound most deeply in the interdomain cleft. A sequence alignment of human and protozoal HGPRTs, which includes secondary structural assignments, is shown in Figure 2.

Purine Binding Specificity

The crystal structure of the human HGPRT−GMP complex showed that the N^2 atom of guanine is hydrogen-bonded to the peptide oxygen atoms of Val187 and Asp193 (Ile200 and Asp206 in *T. gondii* HGPRT; Figure 2), residues that are identical or conservatively substituted in human and protozoal HGPRTs (*10*). This structure suggested, therefore, that the protozoal enzymes must recognize purine bases differently, to accommodate the O^2 atom of xanthine in the active site. In contrast to expectations, our structures of *T. gondii* HGPRT with bound GMP, IMP, and XMP now show that the purine binding interactions of human and protozoal HGPRTs are actually quite similar, and that several subtle structural differences contribute to the productive binding of xanthine by the protozoal enzyme alone. Furthermore, these structural differences that allow the efficient use of xanthine do *not* reside in just one or a few particular amino acids that differ between *T. gondii* and human HGPRT.

Purine Recognition Geometry. Purine bases are recognized in the *T. gondii* HGPRT active site by a convergent array of hydrogen bonds, mostly to main chain atoms, and by several van der Waals interactions. The active site of each nucleotide complex is shown in Figure 3. The human HGPRT−GMP and *T. gondii* $HGPRT_{GMP}$ and $HGPRT_{XMP-PP_i-Mg}$ structures are compared in Figure 4. A schematic view of the $HGPRT_{XMP-PP_i-Mg}$ active site is shown in Figure 3 of the following article (*17*). As seen previously with other HGPRTs, N^7 of the purine is in van der Waals contact with the carboxylate of the catalytic base Asp150. The purine O^6 is coordinated by N^ζ of invariant Lys178 and by the peptide NH of Ile200. In $HGPRT_{GMP}$, the peptide oxygen atom of Ile200 interacts with both the N^1 and N^2 atoms of guanine, with the hydrogen bond to N^1 being somewhat shorter. In $HGPRT_{IMP}$, the hydrogen bond to N^1 is shorter still, whereas in the $HGPRT_{XMP-PP_i-Mg}$ complex, a slight shift of this residue coupled with a slight rotation of the purine ring reduces the extent of the unfavorable interaction between this carbonyl oxygen and xanthine O^2. As seen with human HGPRT (*10*, *12*), guanine N^2 is hydrogen bonded to the peptide oxygen atom of the loop IV residue Asp206. In the xanthine complex, by contrast, a shift of loop IV allows xanthine O^2 to make a hydrogen bond to the Asp206 peptide NH, rather than forming an unfavorable interaction with the peptide oxygen atom. The orientation of all three purine rings is further stabilized on one side by van der Waals interactions with two hydrophobic side chains (Ile148 and Ile200), and on the other side by a π-stacking complex with Trp199. Trp199 N^ϵ also forms a direct ($HGPRT_{IMP}$ and $HGPRT_{XMP-PP_i-Mg}$) or water-mediated ($HGPRT_{GMP}$) hydrogen bond to the Asp206 peptide oxygen atom (Figure 3).

Consistent with the extensive interactions described above, the temperature factors for all three purines are low (~12−17 Å^2), comparable to those of the surrounding protein residues. The opposite was observed in human HGPRT, where the temperature factors for GMP and IMP (~29 and ~45 Å^2) indicated that GMP binds more tightly to that enzyme (*10*, *11*). Measurement of the binding constants for binding of GMP and IMP to human HGPRT (K_D = 7.1 and 61 μM, respectively) supported this crystallographic observation (*11*). The apparently equal binding of these purine rings to *T. gondii* HGPRT is perhaps due to the direct interaction of Trp199 with Asp206, which encases the hypoxanthine ring.

The global interactions of the hood domain residues with the purine bases differ in the three nucleotide complexes. These differences are propagated from loop IV throughout the entire hood domain. First, in the $HGPRT_{IMP}$ and $HGPRT_{XMP-PP_i-Mg}$ complexes, the enzyme grasps the purine ring more tightly than it does in the $HGPRT_{GMP}$ complex. When compared to those of $HGPRT_{GMP}$, loop IV residues

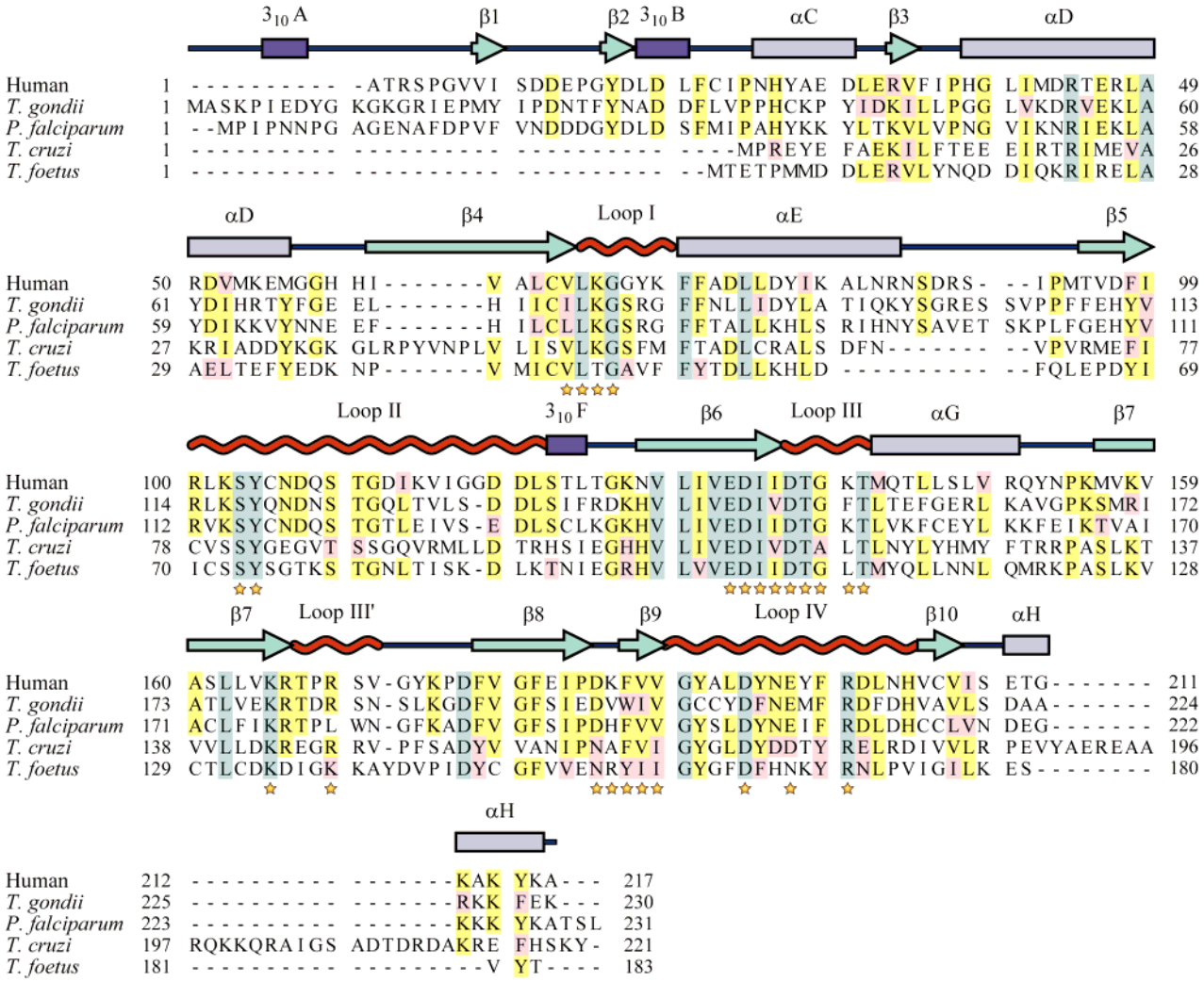

FIGURE 2: Sequence alignment of human and protozoal HGPRTs. The secondary structural elements of *T. gondii* HGPRT (Figure 1) are shown above the sequence, and active site residues are marked with gold stars below the sequence. Absolutely conserved amino acid residues are shaded green, and conservatively substituted residues are shaded yellow (consensus) and pink. The residue numbers for each protein are shown.

203−207 are shifted 1.8 Å toward hypoxanthine or xanthine. Accompanying this shift is an alteration of the φ and ψ angles of the reverse turn residues Cys203 and Cys204, from disfavored regions of the Ramachandran plot ($HGPRT_{GMP}$) into favored regions ($HGPRT_{IMP}$ and $HGPRT_{XMP-PP_i-Mg}$). (The electron density for these two residues in $HGPRT_{GMP}$ is nonetheless unequivocal.) The loop IV shift appears to be brought about in part by the Trp199−Asp206 hydrogen bond. In the absence of this shift, both xanthine and hypoxanthine would be bound very loosely in the active site. In particular, the favorable interaction between xanthine O^2 and the Asp206 peptide NH would be replaced by a repulsive interaction with the peptide oxygen atom. Conversely, were this shift to occur in $HGPRT_{GMP}$, guanine N^2 and the peptide NH would be too closely apposed. Second, in $HGPRT_{GMP}$, residues 208−213 are positioned far from the active site compared to those in the other two complexes; some of the C^α atoms are displaced by more than 3 Å. The closer position adopted in $HGPRT_{IMP}$ and $HGPRT_{XMP-PP_i-Mg}$ is accompanied by a complete reversal of the Arg212 side chain (C^ζ moves 12 Å) that places this side chain in the active site, poised to interact with the pyrophosphate moiety of PRPP (*17*). Third, the C-terminal α-helix of *T. gondii* HGPRT is shifted, moving it 2.2 Å closer to the active site in $HGPRT_{IMP}$ and $HGPRT_{XMP-PP_i-Mg}$ compared to $HGPRT_{GMP}$. All of these structural changes are accommodated by a reshuffling of hydrophobic residues in the hood domain.

Xanthine Recognition Mechanisms. Two structural features contribute to the productive binding of xanthine by *T. gondii* HGPRT. First, the hydrogen bond between Trp199 and Asp206 repositions loop IV such that the Asp206 peptide NH hydrogen bonds to xanthine O^2. This repositioning is reinforced by coordinated motions of the entire hood domain. In *Tritrichomonas foetus* HGPRT, which also uses xanthine efficiently, loop IV is similarly oriented, with Tyr156 O^η (corresponds to Trp199; Figure 2) forming a water-mediated hydrogen bond with Asp163 (*13*). Two facts suggest, however, that the presence of a Trp or Tyr residue at this position is not critical to xanthine use. First, human, *Trypanosoma cruzi*, and *Plasmodium falciparum* HGPRT all have phenylalanine at this position (and thus could not reposition loop IV in this manner), yet *P. falciparum* HGPRT *is* able to use xanthine effectively. Second, the Trp199Phe mutant of *T. gondii* HGPRT has robust xanthine PRTase activity (*42*). Thus, proper positioning of loop IV by Trp199 may contribute to, but is not required for, xanthine PRTase activity. Second, the plasticity of the hood domain's hydrophobic core allows the Ile200 peptide oxygen atom to back

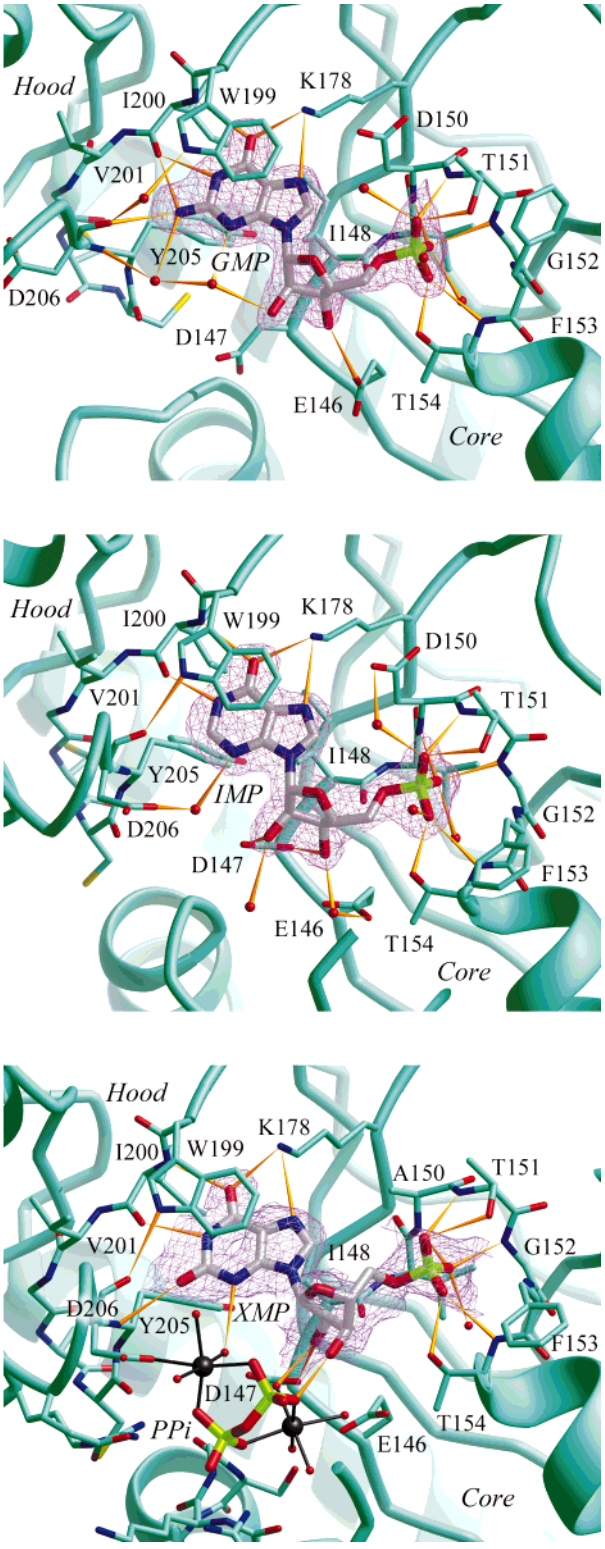

FIGURE 3: Nucleotide interactions in the *T. gondii* HGPRT active site. (Top) $HGPRT_{GMP}$. The protein is shown in a RIBBONS (*41*) representation (green). The hood and core domains are at the top left and bottom right, respectively; loop IV is at the left. The nucleotide is colored by atom type (carbon, silver; nitrogen, blue; oxygen, red; and phosphorus, yellow-green). Water molecules are represented by red spheres, and hydrogen bonds are shown as gold cones. Some water molecules and hydrogen bonds have been omitted for clarity. The omit map electron density for the nucleotide is shown as a lavender net. (Middle) $HGPRT_{IMP}$. (Bottom) $HGPRT_{XMP-PP_i-Mg}$ (*17*). The electron density is a simulated annealing omit map. The pyrophosphate ion and two Mg^{2+} ions (black spheres) are also shown.

away, by 0.1−0.2 Å, from xanthine O^2, thereby mitigating an unfavorable electrostatic interaction between these two atoms. The motion of Ile200 is accompanied by a rotation of xanthine (and hypoxanthine), relative to guanine, by ∼20° away from the Ile200 and Asp206 peptide oxygen atoms.

A previously proposed mechanism for xanthine use is not operative in *T. gondii* HGPRT. It was proposed for *T. foetus* HGPRT that Tyr156 O^{η} could form a *direct* hydrogen bond with xanthine O^2 (*13*). We find no support for such a direct role of N^{ϵ} of Trp199 in *T. gondii* HGPRT, which is positioned more than 3.3 Å from xanthine O^2. Rather, it appears that the aromatic side chain heteroatom hydrogen bonds either through a bridging water molecule or directly to the main chain of Asp206, and thereby helps to place loop IV at the suitable position for guanine versus hypoxanthine or xanthine binding.

Purine Recognition by Human HGPRT. In the absence of crystal structures of human HGPRT bound to xanthine or XMP, it is difficult to conclude unequivocally why this enzyme converts xanthine to product so poorly (*17*). The coordination of GMP by human HGPRT resembles that seen in *T. gondii* $HGPRT_{GMP}$ (*10*, *12*). In addition, the parallelism of purine coordination in $HGPRT_{IMP}$ and $HGPRT_{XMP-PP_i-Mg}$ suggests that human HGPRT, which uses hypoxanthine one-third as efficiently as guanine, should be able to use xanthine far better than it does. Our current working hypothesis is that it is the shifting of the residues in loop IV, particularly the main chain of residues 204−208 (residues 191−195 in human HGPRT), that allows the correct placement of hydrogen bonding partners for the xanthine O^2 versus the guanine N^2 atoms (Figure 4). The required shifts are presumably unfavorable in human HGPRT. We know from our own mutagenesis work that the level of xanthine use by *T. gondii* HGPRT can be dramatically reduced, to a level comparable to that of human HGPRT, by the substitution of residues 199−220 with the corresponding human HGPRT amino acids (*42*). Clearly, these 22 amino acids in the hood domain hinder adoption of a geometry that allows efficient xanthine use, in both human HGPRT and our *T. gondii*−human chimera (*42*). We believe that the detailed packing arrangement of the hydrophobic residues in this region dictates whether the appropriate geometry is easily accessible.

Conformational Changes upon Nucleotide Binding

Purine Binding Site. In the apoenzyme, the purine binding pocket is significantly more open than in the nucleotide complexes (Figure 5). β-Strand 9, which bears Trp199 and Ile200, is shifted by ∼2 Å away from the active site, toward the hood domain. This shift moves Ile200 out of the correct position for making a hydrogen bond to the purine N^1 atom. Furthermore, Trp199 adopts a variety of open conformations in $HGPRT_{Apo}$ (temperature factors of 50−80 $Å^2$) not conducive to purine binding (*16*). In the nucleotide complexes, by contrast, the side chain torsion angles χ^1 and χ^2 of Trp199 are 180° and −90°, respectively, which place the indole ring directly above the purine ring, at a separation of 3.3 Å. In $HGPRT_{Apo}$ compared to the nucleotide complexes, β-strand 6, which bears Ile148, is shifted by ∼1 Å toward the 5′-phosphate binding pocket (loop III). This shift weakens the van der Waals interactions between Ile148 and the

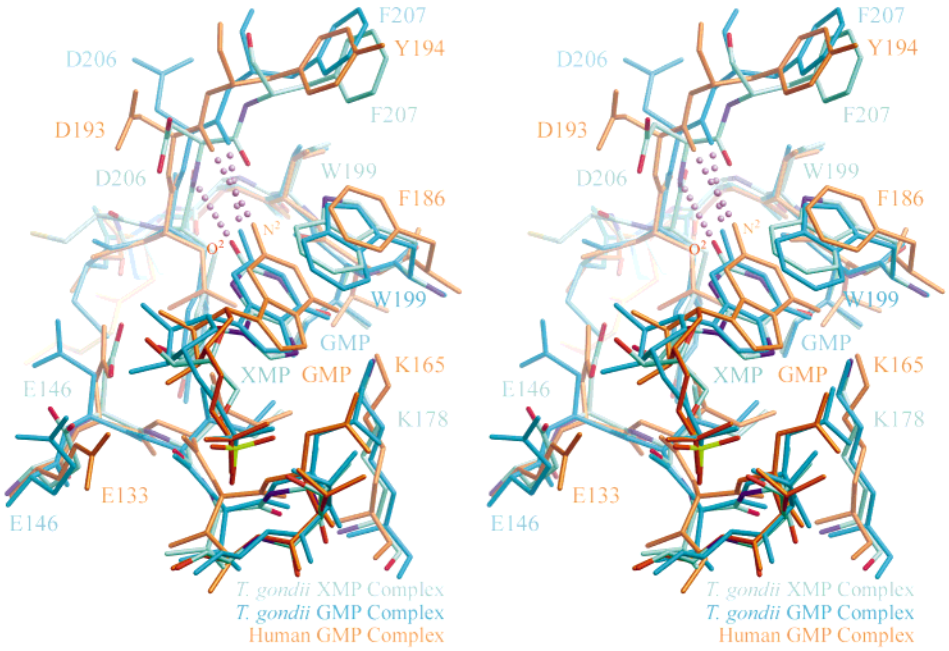

FIGURE 4: Stereoview of the $HGPRT_{GMP}$, $HGPRT_{XMP-PP_i-Mg}$, and human HGPRT−GMP active sites. The view is from loop III (foreground) toward loop IV (background). *T. gondii* $HGPRT_{XMP-PP_i-Mg}$ is shown as color-coded atoms (carbon, sea green), whereas *T. gondii* $HGPRT_{GMP}$ and human HGPRT−GMP (*10*) are cyan and golden-brown, respectively. The key hydrogen bonds that distinguish the XMP complex from the GMP complexes, which connect xanthine O^2 and Asp206 N (XMP), or guanine N^2 and Asp206 (Asp193) O (GMP), are shown as lavender balls.

underside of the purine ring. Thus, the purine ring "clamp" formed by Ile148 and Trp199 is open in the apoenzyme, whereas it is closed in the nucleotide complexes (Figure 5).

5′-Phosphate Binding Site. In the nucleotide complexes, the 5′-phosphate groups of GMP, IMP, and XMP are located in a tight pocket formed by loop III (Asp150−Thr154), which is well-ordered (temperature factors of 20−30 Å^2). The location of the phosphate group, and the conformation of the loop III residues with which it interacts, are essentially identical in the three structures (Figure 3). The three terminal phosphate oxygen atoms are hydrogen bonded to the peptide NHs of loop III, as well as to Thr151 and Thr154 ($O^{\gamma 1}$ atoms) and several water molecules. In stark contrast, loop III is mostly disordered, with temperature factors of 60−100 Å^2, in the apoenzyme (*16*).

Three motions of loop III and the surrounding residues occur upon binding phosphate (Figure 5). First, Val149 (β-strand 6) and Asp150 shift by 1.0 and 1.6 Å, respectively, away from the phosphate, toward β-strand 7. Second, loop III residues Thr151 and Gly152 also shift away from the phosphate, by 2.3 and 1.7 Å, respectively. Finally, the N-terminus of helix G unravels slightly, thereby shifting Thr154 1.9 Å toward the phosphate. The shift of the helix G residues decreases as the distance to the phosphate binding site increases (e.g., Arg161, two turns of helix away, shifts only by 0.65 Å). The motion of the apoenzyme upon binding ribose 5′-phosphate does not alter the overall width of the phosphate binding pocket; the C^α atoms of Asp150 and Thr154 are separated by 8.8 Å in the apoenzyme and 8.9 Å in the nucleotide complexes. Rather, these shifts occur in a coordinated fashion such that the loop assumes a suitable position for receiving the phosphate without distorting its connection to the rest of the nucleotide.

A Fifth Active Site Loop

Previous HGPRT structural studies have established the presence of four active site loops (Figure 1): loop I (residues 78−83 in *T. gondii* HGPRT), which bears a cis peptide bond and plays a key role in binding pyrophosphate; loop II (residues 114−134), the flexible loop which closes over the active site during catalysis; loop III (residues 150−154), which becomes ordered upon binding the 5′-phosphate group of PRPP and nucleotides; and loop IV (residues 202−216), which bears the essential Mg^{2+} ligand, Asp206 (*12*, *15*, *17*). We have found another, previously unrecognized active site loop in HGPRT, loop III′ (residues 180−184).

Loop III′ lies on the surface of the enzyme between β-strands 7 and 8, above and behind loop III (Figure 1). Loop III′ is completely disordered in the HGPRT apoenzyme (*16*). In several subunits of the nucleotide complexes, however, these residues *are* ordered (Figure 6). This ordering places conserved Arg182 (Figure 2) into the active site, where its guanidinium group is sandwiched between the carboxylates of conserved residues Asp150 and Asp197 (Figure 6). In the $HGPRT_{XMP-PP_i-Mg}$ structure, which was determined with a *T. gondii* HGPRT mutant in which Asp150 was mutated to alanine, loop III′ is not ordered, and Arg182 does not interact with Ala150 and Asp197 (*17*). Loop III′ is ordered, however, in several other HGPRT ternary complexes (*12*), including that of *T. gondii* HGPRT with bound PRPP and 9-deazaguanine at 1.05 Å resolution (*43*). We note also that *P. falciparum* HGPRT, the only HGPRT that lacks a basic amino acid corresponding to Arg182 (Figure 2), has a much lower specific activity than *T. gondii* HGPRT, despite the high degree of overall homology between the two enzymes. The role that loop III′ plays in the catalytic mechanism of HGPRT is discussed in the following article (*17*).

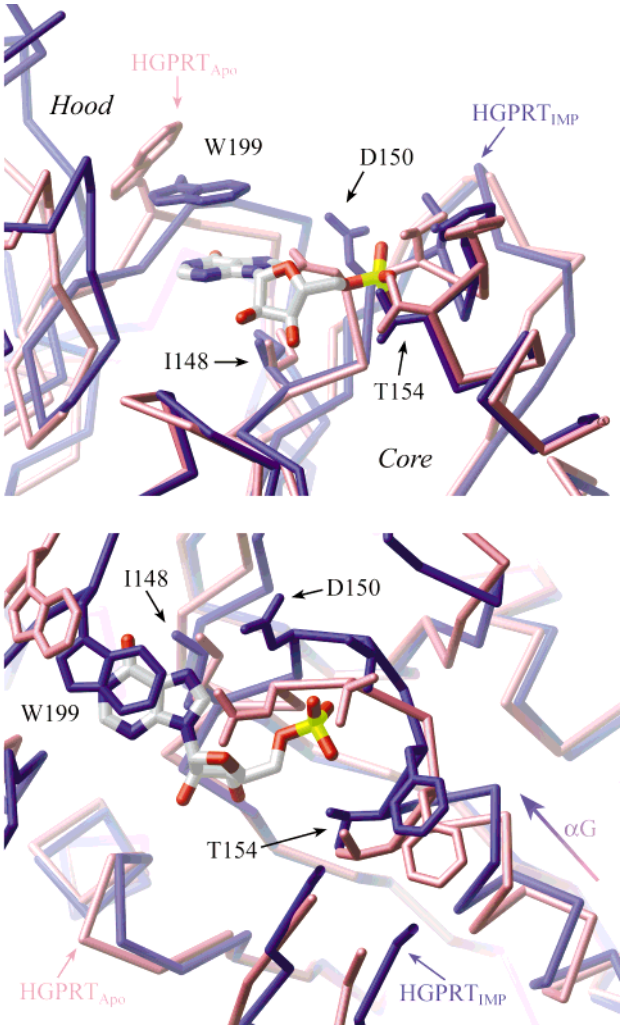

FIGURE 5: Conformational changes that occur upon nucleotide binding to *T. gondii* HGPRT. (Top) The hood domain (top left) of HGPRT$_{Apo}$ (rose) rotates and closes down upon the core domain (bottom right). Trp199 in the apoenzyme adopts a variety of positions, unlike its ordered position closely apposed to IMP as found in HGPRT$_{IMP}$ (blue). In the apoenzyme, Ile148 and Trp199 are separated. In HGPRT$_{IMP}$, these two residues clamp around the purine base. (Bottom) Active site loop III becomes ordered, and it and α-helix G shift (arrow) upon nucleotide binding to cradle the 5′-phosphate group.

Two Isomers of the Leu78−Lys79 Peptide Bond

Like the human HGPRT GMP and IMP complexes (*10*, *11*), in both *T. gondii* HGPRT$_{GMP}$ and HGPRT$_{Apo}$ (*16*), the peptide bond between Leu78 and Lys79 (active site loop I) is in the trans configuration. In HGPRT$_{IMP}$ and HGPRT$_{XMP-PP_i-Mg}$, however, this peptide bond is cis (Figure 7). The cis geometry is also found in the structures of human HGPRT (ternary complex; *12*), *T. cruzi* HGPRT (*14*, *15*), *T. foetus* HGPRT (*13*), and *E. coli* XGPRT (*44*, *45*). The cis peptide bond NH makes an important hydrogen bond to the pyrophosphate moiety in all of these structures; the cis geometry positions Gly80 to hydrogen bond to the pyrophosphate as well. These interactions are not possible when the Leu78−Lys79 peptide bond is in the trans configuration. Indeed, when the peptide is trans the polypeptide chain blocks the binding of PRPP or pyrophosphate. Therefore, it is significant that this peptide bond adopts either the cis or trans configuration, depending on which HGPRT crystal structure is examined.

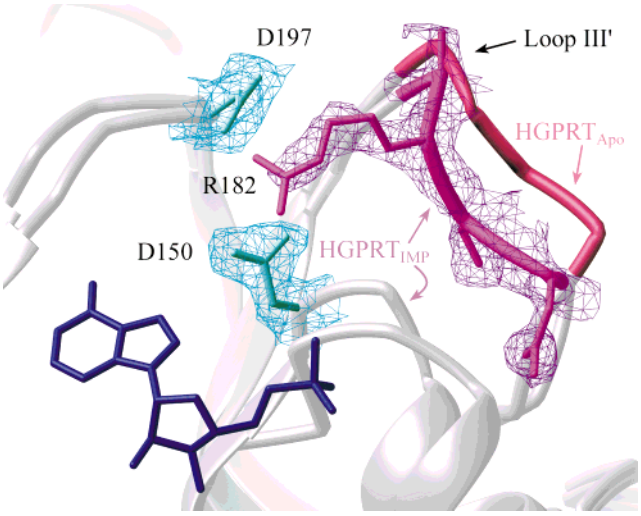

FIGURE 6: Loop III′ binds the hood and core domains together in the upper active site. In HGPRT$_{Apo}$ (rose), loop III′ is disordered. In the nucleotide complexes (HGPRT$_{IMP}$ shown here, magenta), loop III′ becomes ordered, thereby placing Arg182 between Asp150 (core domain) and Asp197 (hood domain). The electron density map for these residues is shown as a net ($2F_o - F_c$, 1σ).

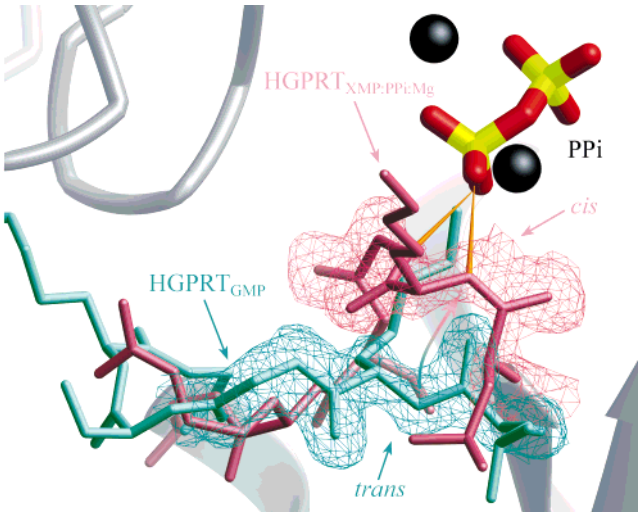

FIGURE 7: Leu78−Lys79 peptide bond in loop I of the *T. gondii* HGPRT active site adopting one of two conformations. The peptide bond is trans in HGPRT$_{GMP}$ (green), whereas it is cis in HGPRT$_{XMP-PP_i-Mg}$ (rose). The simulated annealing omit map electron density for the main chain atoms of residues 78−80 is shown as a net (blue-green and pink, respectively). The peptide nitrogen of Lys79 shifts by 3.8 Å upon isomerization (arrow), thereby adopting a position from which it (and the peptide NH of Gly80) can hydrogen bond (gold cones) to the pyrophosphate ion. Note that the side chain of Lys79 in the trans structure occupies the pyrophosphate binding site.

We excluded the possibility of an incorrect interpretation of the electron density maps in this region. Simulated-annealing omit electron density maps were quite clear (before loop I was added to the models; Figure 7), and the refined temperature factors for the Leu78−Lys79 dipeptide are comparable to those of the rest of the protein, in both the cis HGPRT$_{IMP}$ and HGPRT$_{XMP-PP_i-Mg}$ and the trans HGPRT$_{GMP}$ structures. Examination of the temperature factors for the HGPRT$_{Apo}$ and human HGPRT−GMP structures suggests that these structures are also built correctly in the loop I region.

We considered whether the presence of a cis or trans peptide bond in HGPRT was a consequence of the pH of crystallization. Although human and protozoal HGPRTs have been crystallized over a wide pH range (4.6−8.5), there is no correlation between the pH of crystal growth and the geometric status of this peptide bond. For example, $HGPRT_{Apo}$ and $HGPRT_{GMP}$ (crystals grown at pH 8.45 and 5.0−6.0, respectively) both possess the trans geometry, whereas $HGPRT_{IMP}$ and $HGPRT_{XMP-PP_i-Mg}$ (crystals grown at pH 8.5) both possess the cis geometry.

The possibility that our crystals of *T. gondii* HGPRT [and those of the *T. gondii* HGPRT apoenzyme (*16*) and the human HGPRT nucleotide complexes (*10*, *11*)] may have arisen by the differential crystallization of two non-interconverting populations of the enzyme differing in the geometry of this peptide bond was also considered. We discounted this possibility for several reasons. First, our enzyme is highly active, and different preparations have equivalent specific activities. (Note that the trans isomer must be enzymatically inactive for the reasons discussed above.) So, if there are two populations, with trans inactive, they must be produced in equal amounts in the different preparations, and must copurify. Furthermore, extensive studies of native and recombinant human HGPRT have been performed in many different laboratories. Nonetheless, there has been no indication that two forms of this HGPRT exist, one of which is inactive. In particular, HGPRT is stabilized against heat-induced denaturation in the presence of PRPP (*46*). Only the cis form should be so stabilized, as the trans form of the enzyme could not bind PRPP (*12*, *15*, *17*). To the best of our knowledge, however, heat treatment of (apparently) homogeneous HGPRT has never increased the specific activity of the enzyme. Second, our recombinant enzyme has the expected specific activity, both in comparison with other HGPRTs and in comparison with another group's recombinant *T. gondii* HGPRT, which was purified in a different manner (*19*). Third, the same preparation of enzyme has produced both types (cis and trans) of crystals.

Therefore, we conclude that the Leu78−Lys79 peptide bond of *T. gondii* HGPRT can adopt either the cis or the trans configuration, and that the particular peptide bond geometry is not an artifact of either the protein preparation or the crystallization. We discuss the implications of isomerization of this peptide bond for the HGPRT catalytic mechanism in the following article (*17*).

Exchange of Loop II between HGPRT Active Sites

The suggestion that active site loop II of HGPRT plays an essential role during catalysis (*10*) has been supported by the closed conformation it adopts in HGPRT ternary complex structures (*12*, *15*, *43*). Loop II was disordered in the $HGPRT_{IMP}$ and $HGPRT_{XMP-PP_i-Mg}$ structures, but was ordered for three out of four subunits in the $HGPRT_{GMP}$ structure. In particular, loops II of subunits A and B are closed over each other's active sites (Figure 8). The loops, which adopt a predominantly β-hairpin structure at the end of and perpendicular to β-strand 5, span a distance of 22 Å. They are roughly related by the 2-fold rotation axis between subunits A and B (rms deviation of 2.77 Å, 17 C^{α} atoms). The solvent-accessible surface area buried upon loop II closure (3330 $Å^2$) is very large, a result of many specific

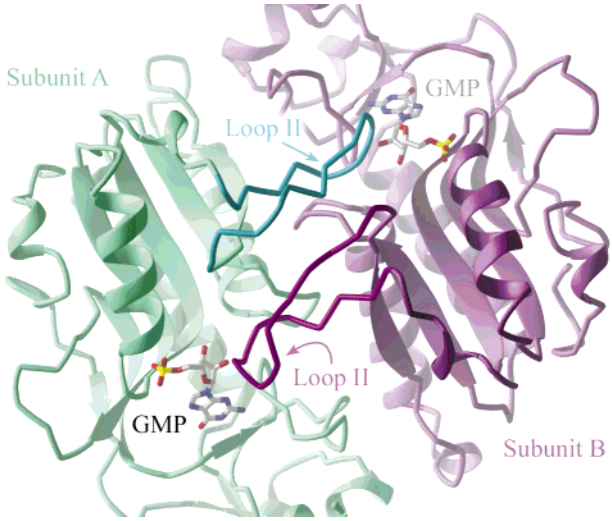

FIGURE 8: Active site loop II exchanges between subunits in $HGPRT_{GMP}$. Loop II of subunit A (green) becomes ordered and extends into the active site of subunit B (lavender). Loop II of subunit B is engaged in a reciprocal exchange. GMP is shown in both active sites.

interactions. The straight β-hairpin conformation observed here is distinct from the bent β-hairpin structure adopted by loop II in the ternary complex structures (*12*, *15*, *43*).

This alternative conformation is another way for flexible loop II of HGPRT to become fully ordered and to close down over the active site. Nonetheless, it is not clear at this point what role, if any, reverse closure of loop II plays in HGPRT catalysis. There is a crystal lattice contact in this region that may affect the ordering of loop II. And, although loop II is closed, it does not completely shelter the active site, as it does in the ternary complex structures (*12*, *15*, *43*). It is extraordinary, however, that loop II *can* close in this alternate manner, for in doing so it prevents loop II of the adjacent subunit from closing productively over its own active site.

ACKNOWLEDGMENT

We thank Dr. Geetha Vasanthakumar for providing the *T. gondii* HGPRT cDNA and the overexpression vector, Sabrina van Ginkel for initial overexpression experiments, and Richard L. Davis for assistance in growing the *E. coli* overproducing strain. We are also grateful for the assistance of Dan Thiel (Cornell High Energy Synchrotron Source) and Mike Soltis (Stanford Synchrotron Radiation Laboratory). We also thank James Sacchettini and Janina Eads for providing coordinates of the human HGPRT−IMP complex. D.W.B. acknowledges the support of the World Health Organization Special Programme for Research and Training in Tropical Diseases (Projects 920170 and 950153) for the study of *P. falciparum* HGPRT. Although this support did not contribute directly to the work presented here, it provided much of the important groundwork that made these studies possible. We especially thank Dr. James R. Piper for his unflagging support of protein crystallography at Southern Research Institute, and for his assistance in the initiation of crystallographic and enzymological studies of *T. gondii* HGPRT by providing support to the early stages of this study from his National Cooperative Drug Discovery Grant (U01-AI30279). The crystallization of the GMP complex was presented in part at the 1995 Annual Meeting of the National

Cooperative Drug Discovery Groups for the Treatment of Opportunistic Infections (Rockville, MD) and at the 1995 Annual Meeting of the American Crystallographic Association (Montréal, PQ). Finally, D.W.B. expresses his heartfelt gratitude to his wife, Julie Bernstein, who has selflessly supported this and other work for many years. Without her support, possible only because she gave up her own successful science career to further his, this work would not have been possible.

REFERENCES

1. Murray, H. W. (1991) in *Harrison's Principals of Internal Medicine* (Wilson, J. D., Braunwald, E., Isselbacher, K. J., Petersdorf, R. G., Martin, J. B., Fauci, A. S., and Root, R. K., Eds.) 12th ed., Chapter 162, pp 795−799, McGraw-Hill, New York.
2. Tuazon, C. U. (1989) *J. Antimicrob. Chemother. 23* (Suppl. A), 77−82.
3. Kovacs, J. A., and Lane, H. C. (1994) *Ann. Intern. Med. 120*, 945−955.
4. Hassan, H. F., and Coombs, G. H. (1988) *FEMS Microbiol. Rev. 54*, 47−84.
5. Krug, E. C., Marr, J. J., and Berens, R. L. (1989) *J. Biol. Chem. 264*, 10601−10607.
6. Wang, C. C. (1984) *J. Med. Chem. 27*, 1−9.
7. Ullman, B., and Carter, D. (1995) *Infect. Agents Dis. 4*, 29−40.
8. Sculley, D. G., Dawson, P. A., Emmerson, B. T., and Gordon, R. B. (1992) *Hum. Genet. 90*, 195−207.
9. Lesch, M., and Nyhan, W. L. (1964) *Am. J. Med. 36*, 561−570.
10. Eads, J. C., Scapin, G., Xu, Y., and Sachettini, J. C. (1994) *Cell 78*, 325−334.
11. Xu, Y., Eads, J., Sacchettini, J. C., and Grubmeyer, C. (1997) *Biochemistry 36*, 3700−3712.
12. Shi, W., Li, C. M., Tyler, P. C., Furneaux, R. H., Grubmeyer, C., Schramm, V. L., and Almo, S. C. (1999) *Nat. Struct. Biol. 6*, 588−593.
13. Somoza, J. R., Chin, M. S., Focia, P. J., Wang, C. C., and Fletterick, R. J. (1996) *Biochemistry 35*, 7032−7040.
14. Focia, P. J., Craig, S. P., III, Nieves-Alicea, R., Fletterick, R. J., and Eakin, A. E. (1998) *Biochemistry 37*, 15066−15075.
15. Focia, P. J., Craig, S. P., III, and Eakin, A. E. (1998) *Biochemistry 37*, 17120−17127.
16. Schumacher, M. A., Carter, D., Roos, D. S., Ullman, B., and Brennan, R. G. (1996) *Nat. Struct. Biol. 3*, 881−887.
17. Héroux, A., White, E. L., Ross, L. J., Davis, R. L., and Borhani, D. W. (1999) *Biochemistry 38*, 14495−14506.
18. Vasanthakumar, G., van Ginkel, S., and Parish, G. (1994) *Gene 147*, 153−154.
19. Donald, R. G. K., Carter, D., Ullman, B., and Roos, D. S. (1996) *J. Biol. Chem. 271*, 14010−14019.
20. Studier, F. W., Rosenberg, A. H., Dunn, J. J., and Dubendorff, J. W. (1990) *Methods Enzymol. 185*, 60−89.
21. Hill, D. L. (1970) *Biochem. Pharmacol. 19*, 545−557.
22. Laemmli, U. K. (1970) *Nature 227*, 680−685.
23. Bradford, M. M. (1976) *Anal. Biochem. 72*, 248−254.
24. Jancarik, J., and Kim, S.-H. (1991) *J. Appl. Crystallogr. 24*, 409−411.
25. Carter, C. W., Jr., and Carter, C. W. (1979) *J. Biol. Chem. 254*, 12219−12223.
26. Collaborative Computational Project, Number 4 (1994) *Acta Crystallogr. D50*, 760−763.
27. Kabsch, W. (1993) *J. Appl. Crystallogr. 24*, 795−800.
28. Leslie, A. G. W. (1992) CCP4 and ESF-EACMB Newsletter on Protein Crystallography 26, Daresbury Laboratory, Warrington, U.K.
29. Evans, P. R. (1997) *Joint CCP4 and ESF-EACBM Newsletter 33*, 22−24.
30. French, S., and Wilson, K. (1978) *Acta Crystallogr. A34*, 517−525.
31. Navaza, J. (1994) *Acta Crystallogr. A50*, 157−163.
32. Tickle, I. J. (1985) in *Molecular Replacement* (Machin, P. A., Ed.) pp 22−26, Daresbury Laboratory, Warrington, U.K.
33. Cowtan, K. (1994) *Joint CCP4 and ESF-EACBM Newsletter on Protein Crystallography 31*, 34−38.
34. Jones, T. A., Zou, J. Y., Cowan, S. W., and Kjelgaard, M. (1991) *Acta Crystallogr. A47*, 110−119.
35. Brünger, A. T., Kuriyan, J., and Karplus, M. (1987) *Science 235*, 458−460.
36. Murshudov, G. N., Vagin, A. A., and Dodson, E. J. (1997) *Acta Crystallogr. D53*, 240−255.
37. Lamzin, V. S., and Wilson, K. S. (1993) *Acta Crystallogr. D49*, 129−147.
38. Laskowski, R. A., MacArthur, M. W., Moss, D. S., and Thornton, J. M. (1993) *J. Appl. Crystallogr. 26*, 283−291.
39. Vriend, G. (1990) *J. Mol. Graphics 8*, 52−56.
40. Hooft, R. W. W., Vriend, G., Sander, C., and Abola, E. E. (1996) *Nature 381*, 272.
41. Carson, M. (1991) *J. Appl. Crystallogr. 24*, 958−961.
42. White, E. L., Ross, L. J., Davis, R. L., Héroux, A., and Borhani, D. W. (1999) (manuscript in preparation).
43. Héroux, A., White, E. L., Ross, L. J., and Borhani, D. W. (1999) (manuscript in preparation).
44. Vos, S., Parry, R. J., Burns, M. R., de Jersey, J., and Martin, J. L. (1998) *J. Mol. Biol. 282*, 875−889.
45. Vos, S., de Jersey, J., and Martin, J. L. (1997) *Biochemistry 36*, 4125−4134.
46. Olsen, A. S., and Milman, G. (1977) *Biochemistry 16*, 2501−2505.

BI990507Q